Institut de Physique du Globe de Paris

Ecole doctorale des Sciences de la Terre

Thèse de Doctorat

pour l'obtention du titre de

Docteur en Science

de l'Institut de Physique du Globe de Paris

Specialité : Geophysique

Soutenue par

Clément Thorey

Magmatisme intrusif sur les planétes telluriques

Équipe Planétologie et Sciences Spatiales,

défendue le 5 Décembre, 2013.

Jury :

Directeur:	Chloé Michaut	-	IPGP (Paris)
Co-directeur:	Mark Wieczorek	-	IPGP (Paris)
Rapporteur :		-	
Rapporteur :		-	
Examinateur :		-	
Examinateur :		-	

Remerciements

Contents

Résumé de la problématique et résultats principaux

Part I

Intrusive magmatism: definition and objective

Chapter 1

Intrusive magmatism – Definition and overview

Chapter 2

Newtonian elastic-plated gravity current

Contents

In this chapter, we sum up the main tentative that have been used to describe the emplacement of magmatic intrusions in the upper crust.

2.1 Theoretical model

At shallow depth in the upper crust, roof lifting is the dominant process by which magma makes room for itself (*Johnson and Pollard*, 1973; *Pollard and Johnson*, 1973), which leads to the deformation and bending of the overlying strata. Such system is commonly modeled as an isoviscous elastic-plated gravity current, i.e. an isoviscous fluid spreading beneath a thin elastic sheet of thickness d_c and above a rigid layer (*Michaut*, 2011; *Bunger and Cruden*, 2011) (Figure 2.1). The behavior of isoviscous elastic-plated gravity current have been largely discussed in the past few years in both carthesian (*Michaut*, 2011; *Bunger and Cruden*, 2011; *Hewitt et al.*, 2014) and axisymmetrical geometry (*Michaut et al.*, 2013; *Lister et al.*, 2013). This section details the results for an axisymmetrical flow which will constitute the reference for more elaborate models in the manuscript.

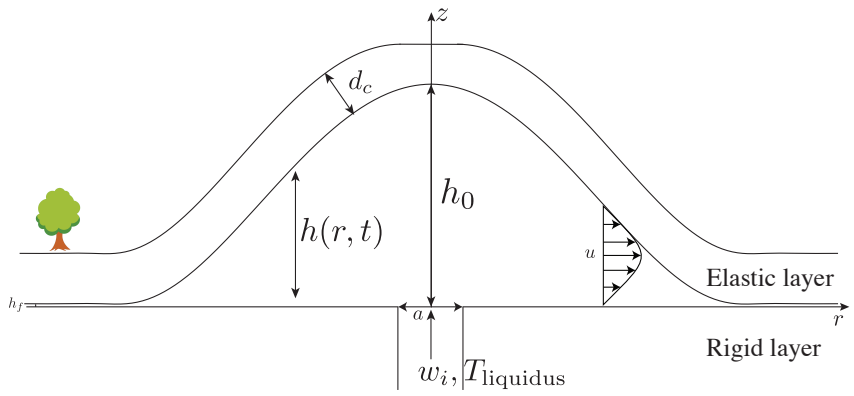

Figure 2.1: Model geometry and parameters.

2.1.1 Velocity field

The intrusion develops over a length scale Λ that is much larger than its thickness H ($\Lambda >> H$). In the laminar regime and in axisymmetrical coordinates (r,z), the Navier-stokes equations within the lubrication assumption are

$$-\frac{\partial P}{\partial r} + \frac{\partial}{\partial z}\left(\eta \frac{\partial u}{\partial z}\right) = 0 \tag{2.1}$$

$$-\frac{\partial P}{\partial z} - \rho_m g = 0 \tag{2.2}$$

where $u(r,z,t)$ the radial velocity, ρ_m the fluid density, η the fluid viscosity, g the standard acceleration due to gravity and $P(r,z,t)$ the pressure within the fluid. Integration of (2.2) thus gives the total pressure $P(r,z,t)$ within the flow. When the vertical deflection deflection $h(r,t)$ of the upper elastic layer is small compared to its thickness d_c, i.e $h << d_c$, we can neglect stretching of the upper layer and only consider bending stresses. Therefore, the total pressure $P(r,z,t)$ at a level z in the intrusion is the sum of four contributions: the weight of the magma and of the upper layer, the bending pressure P_b and the atmospheric pressure P_0

$$P = \rho_m g(h - z) + \rho_r g d_c + P_b + P_0 \tag{2.3}$$

where $h(r,t)$ is the intrusion thickness and ρ_r the density of the surrounding rocks. The bending pressure is given by the force per unit area that is necessary for a vertical displacement h of the thin elastic plate (*Turcotte and Schubert*, 1982)

$$P_d = D\nabla^4 h \tag{2.4}$$

where D is the flexural rigidity of the thin elastic layer, that depends on the Young's modulus E, Poisson's ratio ν^* and on the elastic layer thickness d_c as $D = Ed_c^3/\left(12(1-\nu^*)\right)$. Integration of (2.1) using $\frac{\partial u}{\partial z}\big|_{z=h/2} = 0$ by symmetry

around $h/2$, gives

$$u(r,z,t) = \frac{1}{2}\left(\rho_m g \frac{\partial h}{\partial r} + D\frac{\partial}{\partial r}\left(\nabla^4 h\right)\right) I(z) \tag{2.5}$$

where

$$I(z) = \int_0^z \frac{1}{\eta}\left(2z - h\right) dz \tag{2.6}$$

2.1.2 Injection rate

The effective overpressure ΔP^* driving the flow in the feeder conduit decreases as the intrusion thickens and is given by

$$\Delta P^* = \Delta P - \rho_m g h_0 \tag{2.7}$$

where $h_0(t)$ is the maximum intrusion thickness at the center $r = 0$ and ΔP is the initial driving pressure or the overpressure at the base of the dyke ($z = -Z_c$).

In (2.7), the bending pressure at then center, which scale as $\mathrm{D}h_0(t)/R(t)^4$ where $R(t)$ is the blister radius, has been neglected. Although it tends to infinity at the initiation of the flow, it rapidly vanishes as the blister spreads and the hydrostatic pressure $\rho_m g h_0$ becomes the main contribution to the pressure at the center. In addition, the model assumes a large aspect ratio for the blister and does not consider the initiation of the flow.

Finally, assuming a Poiseuille flow within the cylindrical feeding conduit, the vertical injection velocity $w_i(r,t)$ and injection rate Q_0 are given by

$$w_i = \begin{cases} \frac{\Delta P^*}{4\mu Z_c}\left(\frac{a^2}{4} - r^2\right) & r \leq \frac{a}{2} \\ 0 & r > \frac{a}{2} \end{cases} \tag{2.8}$$

$$Q_0 = \frac{\pi \Delta P^* a^4}{128 \eta Z_c}. \tag{2.9}$$

2.1.3 Governing equations

The fluid is assumed incompressible a global statement of mass conservation gives

$$\frac{\partial h}{\partial t} + \frac{1}{r}\frac{\partial}{\partial r}\left(r\int_0^h u dz\right) = w_i \tag{2.10}$$

Injecting (2.5) and (2.8) into (2.10), we finally get

$$\frac{\partial h}{\partial t} = \frac{1}{2r}\frac{\partial}{\partial r}\left(r\left(\rho_m g \frac{\partial h}{\partial r} + D\frac{\partial}{\partial r}\left(\nabla^4 h\right)\right)\int_0^h I(z) dz\right) + w_i. \tag{2.11}$$

In the case of an isoviscous flow, the integral in (2.11) is easily derived for non-slip boundary condition at the top and the bottom $u(r, z = h, t) = u(r, z = 0, t) = 0$. The equation becomes

$$\frac{\partial h}{\partial t} = \frac{\rho_m g}{12\eta r}\frac{\partial}{\partial r}\left(r h^3 \frac{\partial h}{\partial r}\right) + \frac{D}{12\eta r}\left(r h^3 \frac{\partial}{\partial r}\nabla^4 h\right) + w_i. \tag{2.12}$$

The evolution equation for the flow thickness $h(r,t)$ (2.12) is composed of three different terms on the right hand side. The first term represents gravitational spreading, i.e. spreading of the blister under its own weight. The second term represents the squeezing of the flow by the upper elastic layer. Both term are negative and induces spreading. The last term represents fluid injection and is positive.

2.1.4 Dimensionless equations

Equations (2.8) and (2.12) are nondimensionalized using a horizontal scale Λ, a vertical scale H and a time scale τ given by

$$\Lambda = \left(\frac{D}{\rho_m g}\right)^{1/4} \tag{2.13}$$

$$H = \left(\frac{12\eta Q_0}{\rho_m g \pi}\right)^{\frac{1}{4}} \tag{2.14}$$

$$\tau = \frac{\pi \Lambda^2 H}{Q_0} \tag{2.15}$$

where scales are chosen such that $Q_0 = \pi\Lambda^2 H/\tau$. The length scale represents the flexural wavelength of the upper elastic layer, i.e. the length scale at which bending stresses and gravity contributes equally to flow. The height scale H is the thickness of a typical gravity current and the time scale τ is the characteristic time to fill up a cylindrical flow of radius Λ and thickness H at constant rate Q_0. In addition, we can define a horizontal velocity scale $U = \Lambda/\tau = \left(\rho_m g H^3\right) / \left(12\eta_h \Lambda\right)$.

The dimensionless equation is

$$\frac{\partial h}{\partial t} = \frac{1}{r}\frac{\partial}{\partial r}\left(rh^3\frac{\partial h}{\partial r}\right) + \frac{1}{r}\left(rh^3\frac{\partial}{\partial r}\nabla^4 h\right) + \frac{32}{\gamma^2}\left(\frac{1}{4} - \frac{r^2}{\gamma^2}\right)\left(1 - \frac{h_0}{\sigma}\right) \tag{2.16}$$

where the last term is replaced by zero for $|r| < \gamma/2$.

γ and σ are two dimensionless numbers that control the dynamics of the flow

$$\gamma = \frac{a}{\Lambda} \tag{2.17}$$

$$\sigma = \frac{\Delta P}{\rho_m g h}. \tag{2.18}$$

γ is the dimensionless radius of the conduit, it does not significantly influence the flow and is set to 0.02 in the following (*Michaut and Bercovici*, 2009; *Michaut*, 2011). σ is the normalized pressure head, i.e., the ratio between the initial overpressure driving the flow and the weight of the magma at the center.

Table 2.1: Range of values for the model parameters

Parameters	Symbol	Range of values	Unit
Depth of intrusion	d_c	$0.1 - 5$	km
Young's Modulus	E	$10 - 100$	GPa
Poisson's ratio	ν^*	0.25	
Gravity	g	9.81	m s^{-2}
Magma density	ρ_m	$2800 - 3200$	kg m^{-3}
Magma viscosity	η	$1 - 10^4$	Pa s
Feeder dyke width	a	$10 - 100$	m
Depth of the melt source	Z_c	$200 - 500$	km
Initial overpressure	ΔP	$1 - 20$	MPa
Injection rate	Q_0	$0.1 - 2.10^8$	m^3 s^{-1}
Crust density	ρ_r	2500	kg m^{-3}
Characteristic scales	**Symbol**	**Range of values**	**Unit**
Height scale	H	$1 - 35$	m
Length scale	C	$1 - 50$	km
Time scale	τ	$10^{-3} - 1$	years
Flexural wavelength	Λ	$1 - 12$	km

Table 2.2: Dimensionless numbers

		Complex craters	Simple craters
Symbol	Description	Range of values	Range of values
γ	Normalized source width	$10^{-4} - 10^{-2}$	$10^{-4} - 10^{-2}$
ζ	Normalized wall zone width	$0.05 - 0.13$	0.25
Ψ	Thickening term	$0.3 - 8$	$0.2 - 4$
Ξ	Hydrostatic term	$20 - 400$	$20 - 200$
Θ	Elastic term	$10^{-7} - 0.1$	$10^{-3} - 10$
Ω	Density ratio	1.2	1.2
Φ	Upper layer aspect ratio	4500	1200
σ	Normalized pressure head	$0.6 - 100$	$0.6 - 100$

2.2 Regime of propagations

2.2.1 Bending regime

2.2.2 Gravity current regime

For a constant injection rate, a small pre-wetting film thickness, i.e. $h_f/H << 1$ and a viscosity contrast ν set to 1, $\int_0^h u dz = -h^3 \frac{\partial P}{\partial r}$, the numerical resolution of the equation (3.27) shows two spreading regimes (*Michaut*, 2011; *Bunger and Cruden*, 2011; *Lister et al.*, 2013). At early times, when $R << \Lambda$, gravity is negligible and the dynamics of the spreading is governed by the bending of the upper layer. The spreading is very slow and the interior has uniform pressure $P = \nabla^4 h$. The flow is bell-shaped and its thickness is given by

$$h(r,t) = h_0(t)\left(1 - \frac{r^2}{R^2(t)}\right)^2 \tag{2.19}$$

with $h_0(t)$ the thickness of the intrusion at the center (*Michaut*, 2011; *Lister et al.*, 2013). In this regime, *Lister et al.* (2013) have shown that the spreading is controlled by the propagation of a peeling by bending wave at the intrusion front with dimensionless velocity c

$$c = \frac{\partial R}{\partial t} = h_f^{1/2}\left(\frac{\kappa}{1.35}\right)^{5/2} \tag{2.20}$$

where $\kappa = \partial^2 h/\partial r^2$ is the dimensionless curvature of the interior solution. Using the propagation law (2.20) and the form of the interior solution (2.19), they find that the radius and the height of the intrusion are given by similarity solutions

$$R(t) = 2.2 h_f^{1/22} t^{7/22} \tag{2.21}$$

$$h_0(t) = 0.67 h_f^{-1/11} t^{8/22}. \tag{2.22}$$

where the numerical pre-factor have been matched to our simulations. In addition, the peeling length scale L_p at the front can be quantified in term of the local wave velocity and fluid parameters and follow in a dimensionless form

$$L_p(t) = 1.07 h_f^{13/22} t^{3/22}. \tag{2.23}$$

In contrast, when the radius R becomes larger than Λ ($R >> \Lambda$), the weight of the intrusion becomes dominant over the bending terms. The pressure is given by the hydrostatic pressure $P = h$ and the intrusion enters a classical gravity current regime where bending terms only affect the solution near the intrusion edge (*Huppert*, 1982a; *Michaut*, 2011; *Lister et al.*, 2013). In this second regime, the radius evolves as $t^{1/2}$ and the thickness tends to a constant

$$R(t) = 0.715 t^{1/2} \tag{2.24}$$

$$h_0 = 1.86 \tag{2.25}$$

In the following, we study the effect of the cooling on the blister dynamics in both regime separately for a constant film thickness $h_f = 5 \cdot 10^{-3}$.

2.3 Application to the Earth, Moon and Mars

2.4 Discussion

Part II

Laccolith-sill transitions

Chapter 3

Model for the study of a cooling elastic-plated gravity current

Contents

We present here a general model for the cooling of an elastic-plated gravity current.

3.1 Theory

3.1.1 Formulation

We model an axisymmetric fluid blister of thickness $h(r,t)$ below an elastic layer of constant thickness d_c and above a semi infinite rigid layer (*Michaut*, 2011) (Figure 3.1). The assumption that the thickness of the fluid tends to zero at the contact line leads to divergent viscous stresses, and hence, the theoretical immobility of the blister. To avoid problem at the contact line, we consider a thin pre-wetting film of thickness h_f (*Flitton and King*, 1999; *Lister et al.*, 2013) (Figure 3.1).

The fluid is injected continuously at the base and center of the blister at a rate $Q_0(t)$ through a conduit of diameter a. The hot fluid is intruded at temperature T_i and cools through the top and the bottom by conduction in the surrounding medium, whose temperature T_s is allowed to increase with time.

As it cools, the viscosity of the fluid increases following a prescribed rheology $\eta(T)$ bounded between two values: the viscosity of the hottest fluid η_h at temperature T_i and the viscosity of the coldest fluid η_c at temperature T_0.

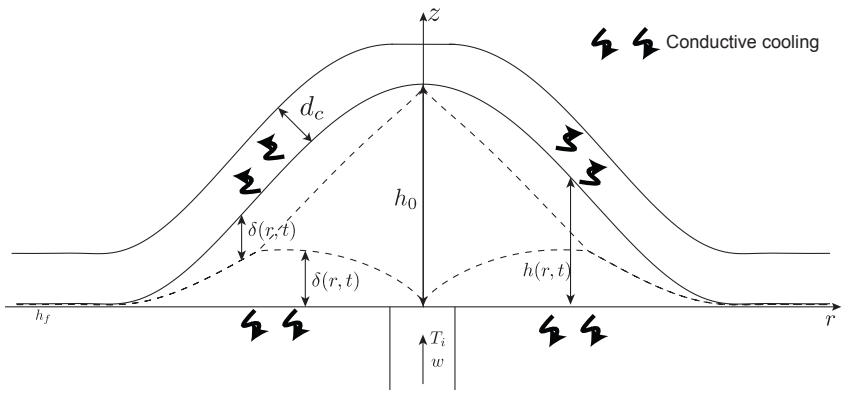

Figure 3.1: Model geometry and parameters.

3.1.2 Velocity field

The intrusion develops over a length scale Λ that is much larger than its thickness H ($\Lambda >> H$). In the laminar regime and in axisymmetrical coordinates (r,z), the Navier-stokes equations within the lubrication assumption are

$$-\frac{\partial P}{\partial r} + \frac{\partial}{\partial z}\left(\eta(T)\frac{\partial u}{\partial z}\right) = 0 \tag{3.1}$$

$$-\frac{\partial P}{\partial z} - \rho_m g = 0 \tag{3.2}$$

where $u(r,z,t)$ the radial velocity, ρ_m the fluid density, g the standard acceleration due to gravity and $P(r,z,t)$ the pressure within the fluid. Integration of (3.2) thus gives the total pressure $P(r,z,t)$ within the flow. When the vertical deflection deflection $h(r,t)$ of the upper elastic layer is small compared to its thickness d_c, i.e $h << d_c$, we can neglect stretching of the upper layer and only consider bending stresses. Therefore, the total pressure $P(r,z,t)$ at a level z in the intrusion is the sum of three contributions: the weight of the magma and of the upper layer and the bending pressure

$$P = \rho_m g(h-z) + \rho_r g d_c + D\nabla^4 h \tag{3.3}$$

where $h(r,t)$ is the intrusion thickness, ρ_r the density of the surrounding rocks and D is the flexural rigidity of the thin elastic layer, that depends on the Young's modulus E, Poisson's ratio ν^* and on the elastic layer thickness d_c as $D = Ed_c^3/12(1-\nu^*)$. Integration of (3.1) using $\frac{\partial u}{\partial z}\big|_{z=h/2} = 0$ by symmetry around $h/2$, gives:

$$u(r,z,t) = \frac{1}{2}\left(\rho_m g\frac{\partial h}{\partial r} + D\frac{\partial}{\partial r}\left(\nabla_r^2\left(\nabla_r^2 h(r)\right)\right)\right)\int_0^z \frac{1}{\eta(T)}\left(2z-h\right)dz \tag{3.4}$$

3.1.3 Injection rate

Assuming a Poiseuille flow within the cylindrical feeding conduit, the vertical injection velocity $w(r,t)$ and injection rate Q_0 are given by:

$$w(r,t) = \begin{cases} \frac{\Delta P}{4\mu Z_c}\left(\frac{a^2}{4} - r^2\right) & r \leq \frac{a}{2} \\ 0 & r > \frac{a}{2} \end{cases} \tag{3.5}$$

$$Q_0 = \frac{\pi \Delta P a^4}{128 \mu Z_c} \tag{3.6}$$

where ΔP is the initial overpressure within the melt at $z = Z_c$. The fluid is injected at the liquidus temperature T_i.

3.1.4 Heat transport equation

3.1.4.1 Local energy conservation

In the laminar regime and in axisymmetrical coordinates (r,z), the local energy conservation equation within the lubrication assumption is written as

$$\frac{D}{Dt}\left(\rho_m C_{p,m} T + \rho_m L(1-\phi)\right) = k_m \frac{\partial^2 T}{\partial z^2} \tag{3.7}$$

where $T(r,z,t)$ is the fluid temperature, $\phi(r,z,t)$ is the crystal fraction in the melt and ρ_m, k_m, $C_{p,m}$ and L are the density, thermal conductivity, specific heat and latent heat of the fluid. In this model, the crystals are considered only as a source/sink of energy as they melt/form during the flow emplacement. In particular, they share the same properties that the fluid itself.

Following a common approximation, we assume that the crystal fraction is a linear function of temperature over the melting interval

$$\phi = \frac{T_L - T}{T_L - T_s} \tag{3.8}$$

where T_S and T_L are the solidus and liquidus temperatures of the magma (*Hort*, 1997; *Michaut and Jaupart*, 2006). With this approximation, the local energy equation (3.7) resumes to

$$\frac{\partial T}{\partial t} + u\frac{\partial T}{\partial r} + w\frac{\partial T}{\partial z} = \frac{\kappa_m}{1 + St^{-1}} \frac{\partial^2 T}{\partial z^2} \tag{3.9}$$

where $u(r,z,t)$ and $w(r,z,t)$ are the radial and vertical fluid velocities, $St = \left(C_{p,m}(T_L - T_S)\right)/L$ is the Stephan number and κ_m is the fluid thermal diffusivity $\kappa_m = k_m/\rho_m C_{p,m}$. Following *Balmforth and Craster* (2000), we use an integral balance method to solve the heat transport equation (3.9). This theory is based on the integral-balance method of heat-transfer theory of *Goodman* (1958), in which the vertical structure of the temperature field is represented by a known function of depth that approximates the expected solution.

3.1.4.2 Integral balance solution for the temperature $T(r,z,t)$

We model the cooling of the fluid blister through the growth of two thermal boundary layers: one growing downward from the top and a second growing upward from the base. As we consider homogeneous thermal properties for the surrounding rocks, we assume that the two thermal boundary layers grow symmetrically and have the same thickness $\delta(r,t)$. In agreement, the integral-balance approximation we use for the vertical temperature profile $T(r,z,t)$ is

$$T = \begin{cases} T_b - (T_b - T_s)(1 - \frac{z}{\delta})^2 & 0 \leq z \leq \delta \\ T_b & \delta \leq z \leq h - \delta \\ T_b - (T_b - T_s)(1 - \frac{h-z}{\delta})^2 & h - \delta \leq z \leq h \end{cases} \tag{3.10}$$

where $T_b(r,t)$ is the temperature at the center of the flow and $T_s(r,t)$ the temperature at the contact with the surrounding rocks (Figure 3.1). The integral balance solution in (3.10) assumes a symmetry around $z = h/2$ and a decrease of the temperature in the two thermal boundary layers down to the surrounding rock temperature T_s (*Balmforth and Craster*, 2000). In addition, it assumes a uniform temperature T_b in between the thermal boundary layers. Then, as the fluid is injected at a temperature T_i, we have $T_b(r,t) = T_i$ when $\delta < h/2$. However, if the two thermal boundary layers connect, then $\delta = h/2$ and T_b decreases such that $T_b \leq T_i$.

3.1.4.3 Integral balance equation

We begin by integrating the local energy conservation (3.9) over the two thermal boundary layers. The integration over the bottom thermal layer, i.e. from the base, $z = 0$ to a level $z = \delta$ gives

$$\begin{aligned} &\frac{\partial}{\partial t}\left(\delta(\bar{T} - T_b)\right) + \frac{1}{r}\frac{\partial}{\partial r}\left(r\delta(\overline{uT} - \bar{u}T_b)\right) + \delta\left(\frac{\partial T_b}{\partial t} + \bar{u}\frac{\partial T_b}{\partial r}\right) \\ = \; & -\frac{\kappa_m}{1 + St^{-1}}\left.\frac{\partial T}{\partial z}\right|_{z=0} + w_{inj}(T_i - T_b) \end{aligned} \tag{3.11}$$

where the bar indicate the vertical average over the bottom thermal boundary layer

$$\overline{f} = \frac{1}{\delta}\int_0^\delta f dz,$$

$T_b(r,t)$ is the temperature at $z = \delta$, $w_{inj}(r)$ is the vertical injection velocity and we have used the nullity of the thermal gradient at $z = \delta$ and the local mass conservation

$$\frac{1}{r}\frac{\partial ru}{\partial r} + \frac{\partial w}{\partial z} = 0. \tag{3.12}$$

The integration over the top thermal layer, i.e., from the level, $z = h - \delta$ to the top $z = h$ gives:

$$\begin{aligned} &\frac{\partial}{\partial t}\left(\delta(\bar{T} - T_b)\right) + \frac{1}{r}\frac{\partial}{\partial r}\left(r\delta(\overline{uT} - \bar{u}T_b)\right) + \delta\left(\frac{\partial T_b}{\partial t} + \bar{u}\frac{\partial T_b}{\partial r}\right) \\ = \; & \frac{\kappa_m}{1 + St^{-1}}\left.\frac{\partial T}{\partial z}\right|_{z=h}. \end{aligned} \tag{3.13}$$

where, in addition to the local mass conservation (3.12) and the fact the thermal gradient at $z = h-\delta$ is equal to zero, we have used the kinematic boundary condition in $z = h(r,t)$

$$\frac{\partial h}{\partial t} + u\frac{\partial h}{\partial r} = w \tag{3.14}$$

The heat balance equation can then be written by adding (3.11) and (3.13) and introducing (3.10)

$$\begin{aligned} &\frac{\partial}{\partial t}\left(\delta(\bar{T}-T_b)\right) + \frac{1}{r}\frac{\partial}{\partial r}\left(r\delta(\overline{uT}-\bar{u}T_b)\right) + \delta\left(\frac{\partial T_b}{\partial t} + \overline{u}\frac{\partial T_b}{\partial r}\right) \\ = \;& \frac{\kappa_m}{2(1+St^{-1})}\left(\left.\frac{\partial T}{\partial z}\right|_{z=h} - \left.\frac{\partial T}{\partial z}\right|_{z=0}\right) + \frac{w_{inj}}{2}(T_i - T_b) \end{aligned} \tag{3.15}$$

3.1.4.4 Thermal boundary conditions

At the contact with the surrounding rock, the heat is lost by conduction:

$$k_m \left.\frac{\partial T}{\partial z}\right|_{z=0} = k_r \left.\frac{\partial T_r}{\partial z}\right|_{z=0} \tag{3.16}$$

$$k_m \left.\frac{\partial T}{\partial z}\right|_{z=h} = k_r \left.\frac{\partial T_r}{\partial z}\right|_{z=h} \tag{3.17}$$

where $T_r(r,z)$ is the temperature in the surrounding medium. Assuming a semi infinite layer for the rigid layer below the intrusion, *Carslaw and Jaeger* (1959) show that the temperature T_r in the surrounding rocks can be approximated to a first order by

$$T_r(r,z,t) - T_0 = (T_s - T_0)\,\mathrm{erfc}\left(\frac{-z}{2\sqrt{\kappa_r t}}\right). \tag{3.18}$$

The thickness of the upper layer is equal to the intrusion depth d_c. However, we assume that the depth d_c is large compared to the characteristic length scale for conduction L_c and we use the same approximation to derive T_r above the intrusion

$$T_r(r,z,t) - T_0 = (T_s - T_0)\,\mathrm{erfc}\left(\frac{z-h}{2\sqrt{\kappa_r t}}\right). \tag{3.19}$$

Therefore, the two thermal boundary conditions (3.16) and (3.17) become:

$$k_m \left.\frac{\partial T}{\partial z}\right|_{z=0} = k_r \frac{T_s - T_0}{\sqrt{\pi\kappa_r t}} \tag{3.20}$$

$$k_m \left.\frac{\partial T}{\partial z}\right|_{z=h} = -k_r \frac{T_s - T_0}{\sqrt{\pi\kappa_r t}} \tag{3.21}$$

3.1.5 Dimensionless equations

A global statement of mass conservation gives the evolution of the thickness (*Huppert*, 1982a; *Michaut*, 2011)

$$\frac{\partial h}{\partial t} + \frac{1}{r}\frac{\partial}{\partial r}\left(r\int_0^h u dz\right) = w_{inj}. \tag{3.22}$$

This equation is then coupled to the heat-balance equation (3.15) through the viscosity dependence, which itself depends on temperature, of the velocity (3.4). We first rewrite the different temperatures such that $T = T_0 + (T_i - T_0)\theta$ where $\theta(r, z, t)$ is the equivalent dimensionless temperature. In term of θ, the integral balance approximation (3.10) rewrites

$$\theta(z) = \begin{cases} \Theta_b - (\Theta_b - \Theta_s)\,(1 - \frac{z}{\delta})^2 & 0 \leq z \leq \delta \\ \Theta_b & \delta \leq z \leq h - \delta \\ \Theta_b - (\Theta_b - \Theta_s)\,(1 - \frac{h-z}{\delta})^2 & h - \delta \leq z \leq h \end{cases} \tag{3.23}$$

where $\Theta_b = \frac{T_b - T_0}{T_i - T_0}$ and $\Theta_s = \frac{T_s - T_0}{T_i - T_0}$. Equations (3.4), (3.15) and (3.22) are nondimensionalized using a horizontal scale Λ, a vertical scale H and a time scale τ given by (*Michaut*, 2011; *Michaut et al.*, 2013; *Michaut and Manga*, 2014; *Thorey and Michaut*, 2014)

$$\Lambda = \left(\frac{D}{\rho_m g}\right)^{1/4} \tag{3.24}$$

$$H = \left(\frac{12\eta_h Q_0}{\rho_m g \pi}\right)^{\frac{1}{4}} w \tag{3.25}$$

$$\tau = \frac{\pi \Lambda^2 H}{Q_0} \tag{3.26}$$

where Λ represents the flexural wavelength of the upper elastic layer (*Michaut*, 2011), H the thickness of a typical gravity current (*Huppert*, 1982b) and τ the characteristic time to fill up a cylindrical flow of radius Λ and thickness H at constant rate Q_0. In addition, we can define a horizontal velocity scale $U = \Lambda/\tau = \left(\rho_m g H^3\right) / \left(12\eta_h \Lambda\right)$.

The dimensionless equations are

$$\frac{\partial h}{\partial t} = -\frac{1}{r}\frac{\partial}{\partial r}\left(r\int_0^h u dz\right) + w_{inj} \tag{3.27}$$

$$\begin{aligned} \frac{\partial}{\partial t}\left(\delta(\bar{\theta} - \Theta_b)\right) &= -\frac{1}{r}\frac{\partial}{\partial r}\left(r\delta(\overline{u\theta} - \bar{u}\Theta_b)\right) - \delta\left(\frac{\partial \Theta_b}{\partial t} + \bar{u}\frac{\partial \Theta_b}{\partial r}\right) - 2Pe^{-1}St_m\frac{(\Theta_b - \Theta_s)}{\delta} \\ &+ \frac{w_{inj}}{2}(1 - \Theta_b) \end{aligned} \tag{3.28}$$

$$u = 6\left(\frac{\partial h}{\partial r} + \frac{\partial}{\partial r}\nabla^2 h\right)\int_0^z \frac{1}{\eta^*(\theta, \nu)}\,(2z - h)\,dz \tag{3.29}$$

$$w_{inj} = \frac{32}{\gamma^2}\left(\frac{1}{4} - \frac{r^2}{\gamma^2}\right) \quad \text{if } r < \gamma/2 \tag{3.30}$$

where $\eta^*(\theta, \nu)$ is the dimensionless rheology η/η_h and the thermal boundary conditions (3.20) and (3.21) resume to

$$2\frac{\Theta_b - \Theta_s}{\delta} = \Omega Pe^{1/2}\frac{\Theta_s}{\sqrt{\pi t}}. \tag{3.31}$$

γ, Pe, St_m, ν and Ω are the five dimensionless numbers that control the dynamics of the flow

$$\gamma = \frac{a}{\Lambda} \tag{3.32}$$

$$Pe = \frac{H^2}{\kappa_m \tau} \tag{3.33}$$

$$St_m = \frac{C_{p,m}\left(T_L - T_S\right)}{C_{p,m}\left(T_L - T_S\right) + L} \tag{3.34}$$

$$\nu = \frac{\eta_h}{\eta_c} \tag{3.35}$$

$$\Omega = \frac{k_r}{k_m}\left(\frac{\kappa_m}{\kappa_r}\right)^{1/2} \tag{3.36}$$

γ is the dimensionless radius of the conduit, it does not significantly influence the flow and is set to 0.02 in this study (*Michaut and Bercovici*, 2009; *Michaut*, 2011), Pe is the Peclet number, it compares the vertical diffusion of heat to the horizontal advection in the intrusion interior, St_m is a modified Stephan number, it is the ratio of sensible heat between solidus and liquidus to the total energy of the fluid at liquidus temperature, ν is the maximum viscosity contrast, i.e. the ratio between the hottest and coldest viscosity and and Ω is the ratio between heat conduction at the contact with the encasing rocks and heat diffusion within the fluid.

3.1.6 Further simplifications and final equations

The heat balance equations (3.28) can reduce to

$$\frac{\partial}{\partial t}\left(\delta(\bar{\theta} - 1)\right) + \frac{1}{r}\frac{\partial}{\partial r}\left(r\delta(\overline{u\theta} - \bar{u})\right) = -2Pe^{-1}St_m\frac{(\Theta_b - \Theta_s)}{\delta} \tag{3.37}$$

Indeed, if the thermal boundary layers exist, $\Theta_b = 1$, δ is the variable and the heat balance equation (3.28) reduces to the equation (3.37). In contrast, if the thermal boundary layers merge, $\delta = h/2$ and the variable is Θ_b. In this case, the heat balance equations (3.28) reduces to:

$$\frac{\partial h\bar{\theta}}{\partial t} + \frac{1}{r}\frac{\partial}{\partial r}\left(rh\overline{u\theta}\right) - \Theta_b\left(\frac{\partial h}{\partial t} + \frac{1}{r}\frac{\partial}{\partial r}\left(rh\bar{u}\right)\right) = -8St_m Pe^{-1}\frac{(\Theta_b - \Theta_s)}{h} + w_{inj}(1 - \Theta_b)$$

which we can rewrite using (3.27) as

$$\frac{\partial h\bar{\theta}}{\partial t} + \frac{1}{r}\frac{\partial}{\partial r}\left(rh\overline{u\theta}\right) = w_i - 8St_m Pe^{-1}\frac{(\Theta_b - \Theta_s)}{h}$$

which also corresponds to (3.37) in the case where $\delta = h/2$.

Following *Balmforth and Craster* (2000), we rewrite (3.37) using a new variable $\xi = \delta(1-\overline{\theta})$

$$\frac{\partial \xi}{\partial t} + \frac{1}{r}\frac{\partial}{\partial r}\left(r\bar{u}\xi\right) - \frac{1}{r}\frac{\partial}{\partial r}\left(r\delta(\overline{u\theta} - \bar{u}\bar{\theta})\right) = 2Pe^{-1}St_m\frac{(\Theta_b - \Theta_s)}{\delta} \tag{3.38}$$

This equation contains advection by the vertically integrated radial velocity, with a correction accounting for the vertical structure of the temperature field and conduction cooling. The system composed by (3.27) and (3.38), whose main variable are h and ξ is complete. Indeed, the temperature at the contact with the surrounding Θ_s is built from the variable ξ

$$\Theta_s(r,t) = \begin{cases} \frac{3\beta}{4}\xi - \frac{\sqrt{3}}{4}\sqrt{\beta\xi\left(3\beta\xi+8\right)} + 1 & \text{if} \quad \xi \leq \xi_t \\ \frac{-12\xi+6h(r,t)}{(\beta h(r,t)+6)h(r,t)} & \text{if} \quad \xi > \xi_t \end{cases} \tag{3.39}$$

where

$$\xi_t(t) = \frac{\beta(t)h^2(r,t)}{6\beta(t)h(r,t)+24} \tag{3.40}$$

$$\beta(t) = \Omega Pe^{1/2}\frac{1}{\sqrt{\pi t}} \tag{3.41}$$

which leads to the expression of Θ_b and δ

$$\Theta_b(r) = \begin{cases} 1 & \text{if} \quad \xi \leq \xi_t \\ \frac{\Theta_s}{4}\left(\beta(t)h(r,t)+4\right) & \text{if} \quad \xi > \xi_t \end{cases} \tag{3.42}$$

$$\delta(r) = \begin{cases} \frac{1}{\Theta_s\beta(t)}\left(-2\Theta_s+2\right) & \text{if} \quad \xi \leq \xi_t \\ h(r,t)/2 & \text{if} \quad \xi > \xi_t \end{cases} \tag{3.43}$$

Equations (3.27) and (3.38) are solved numerically using the Newton-Raphson method which leads to a second-order scheme in time and space. In all solutions, we computed the mass and energy conservation as a test for the accuracy of the convergence.

3.2 Numerical approach

3.2.1 Equation on the thickness

3.2.2 Heat transport equation

3.2.3 Convergence

Chapter 4

First order modelling - Isothermal rocks

Chapter 5

Floor fractured craters on the Moon

Part III

Floor-fractured craters

Chapter 6

Floor fractured craters on the Moon

Chapter 7

Gravitationnal signature of Floor-fractured craters

Chapter 8

New detection using machine learning techniques

Bibliography

Balmforth, N. J., and R. V. Craster (2000), Dynamics of cooling domes of viscoplastic fluid, *J. Fluid Mech.* (Cited on pages 19, 20 and 24.)

Bunger, A. P., and A. R. Cruden (2011), Modeling the growth of laccoliths and large mafic sills: Role of magma body forces, *J. Geophys. Res.*, *116*(B2), B02,203. (Cited on pages 7 and 12.)

Carslaw, H. S., and J. C. Jaeger (1959), Heat in solids. (Cited on page 21.)

Flitton, J. C., and J. R. King (1999), Moving-boundary and fixed-domain problems for a sixth-order thin-film equation, *15*(6), 713–754. (Cited on page 17.)

Goodman, T. R. (1958), *The heat-balance integral and its application to problems involving a change of phase*, Trans. ASME. (Cited on page 19.)

Hewitt, I. J., N. J. Balmforth, and J. R. De Bruyn (2014), Elastic-plated gravity currents, pp. 1–29. (Cited on page 7.)

Hort, M. (1997), Cooling and crystallization in sheet-like magma bodies revisited, *Journal of Volcanology and Geothermal Research*, *76*(3-4), 297–317. (Cited on page 19.)

Huppert, H. E. (1982a), The propagation of two-dimensional and axisymmetric viscous gravity currents over a rigid horizontal surface, *J. Fluid Mech.*, *121*(-1), 43–58. (Cited on pages 12 and 22.)

Huppert, H. E. (1982b), Flow and instability of a viscous current down a slope, *Nature*. (Cited on page 22.)

Johnson, A. M., and D. D. Pollard (1973), Mechanics of growth of some laccolithic intrusions in the Henry mountains, Utah, I: field observations, Gilbert's model, physical properties and flow of the magma, *Tectonophysics*. (Cited on page 7.)

Lister, J. R., G. G. Peng, and J. A. Neufeld (2013), Viscous Control of Peeling an Elastic Sheet by Bending and Pulling, *Phys. Rev. Lett.*, *111*(15), 154,501. (Cited on pages 7, 12 and 17.)

Michaut, C. (2011), Dynamics of magmatic intrusions in the upper crust: Theory and applications to laccoliths on Earth and the Moon, *J. Geophys. Res.*, *116*(B5), B05,205. (Cited on pages 7, 10, 12, 17, 22 and 23.)

Michaut, C., and D. Bercovici (2009), A model for the spreading and compaction of two-phase viscous gravity currents, *J. Fluid Mech.*, *630*, 299–329. (Cited on pages 10 and 23.)

Michaut, C., and C. Jaupart (2006), Ultra-rapid formation of large volumes of evolved magma, *Earth and Planetary Science Letters*, *250*(1-2), 38–52. (Cited on page 19.)

Michaut, C., and M. Manga (2014), Domes, pits, and small chaos on Europa produced by water sills, *J. Geophys. Res. Planets*, *119*(3), 550–573. (Cited on page 22.)

Michaut, C., D. Baratoux, and C. Thorey (2013), Magmatic intrusions and deglaciation at mid-latitude in the northern plains of Mars, *Icarus*, *225*(1), 602–613. (Cited on pages 7 and 22.)

Pollard, D. D., and A. M. Johnson (1973), Mechanics of growth of some laccolithic intrusions in the Henry Mountains, Utah, II: bending and failure of overburden layers and sill formation, *Tectonophysics*, *18*(3-4), 311–354. (Cited on page 7.)

Thorey, C., and C. Michaut (2014), A model for the dynamics of crater-centered intrusion: Application to lunar floor-fractured craters, *J. Geophys. Res. Planets*, *119*(1), 286–312. (Cited on page 22.)

Turcotte, D. L., and G. Schubert (1982), Geodynamics: Applications of continuum physics to geological problems, John Wiley, New York. (Cited on page 8.)